26th ABCM International Congress of Mechanical Engineering
November 22-26, 2021. Florianópolis, SC, Brazil

COBEM2021-0115
EFFECT OF MACHINING PARAMETERS ON CUTTING FORCES DURING THE END MILLING OF UNS S32205

Júlia Caniçali[1]
Eduardo Sperotto[2]
Maurício R. Policena[3]
André J. Souza[4]

Federal University of Rio Grande do Sul (UFRGS) – Department of Mechanical Engineering (DEMEC)
Laboratory of Automation in Machining (LAUS) – 90050-170 – Porto Alegre, RS – Brazil.

[1]juliacanicali@hotmail.com; [2]eduardo_sperotto@hotmail.com [3]mrpolicena@gmail.com; [4]ajsouza@ufrgs.br

Abstract. *Duplex stainless steel (DSS) is a low-machinability alloy with a biphasic structure (50% ferrite and 50% austenite) applied in oil tanker tanks, pulp and paper industries, digesters, valves, flanges, and pipes. The tool alternates cutting between soft and hard grain during the machining, leaning to initiate a self-excited vibration. Moreover, a greater cutting force in the feed direction is produced on DSS machining due to its lower ductility and high tensile strength at high temperatures. Thus, this work investigated the influence of machining parameters [cutting speed (v_c), feed per tooth (f_z), axial depth of cut (a_p), and tool nose radius (r_ε)] on the static (μF) and dynamic (ΔF) portions of the active (F_a) and passive (F_p) machining force components in the flood end milling of UNS S32205. The response variables ($\mu F_a \pm \Delta F_a$ and $\mu F_p \pm \Delta F_p$) were analyzed through the Box-Behnken experimental design. The analysis of variance showed that r_ε, a_p/r_ε and f_z were the most significant input parameters over the response variables. After the multivariate optimization, the lower values of F_a and F_p were generated using a higher value of v_c (110 m/min) and lower values of r_ε (0.4 mm) and a_p (0.2 mm), with low f_z (0.0724 mm/tooth.*

Keywords: *duplex stainless steel, end milling, active and passive force components, static and dynamic portions, Box-Behnken Design.*

1. INTRODUCTION

Duplex stainless steels (DSS) are Fe-Cr-Ni alloys formed by a two-phase microstructure, composed of a ferritic matrix (Fe-α) and austenite islands (Fe-γ) precipitated and morphologically rounded, with volume fractions of approximately 50% each phase, which combines high resistance to corrosion in aggressive media with high mechanical resistance. These are alloys with a chromium percentage between 20-30%, nickel between 5-10%, and very low carbon contents (less than 0.03%) to avoid Cr_3C_2 precipitation. As a result, these carbides act as preferred sites for pitting corrosion. The high content of Cr improves corrosion resistance by forming the passive layer. However, with progressive increases in Cr (ferrite stabilizer), there is a precipitation of a Fe-σ phase that results in loss of ductility, toughness, and corrosion resistance. The high nickel content results in a higher Fe-γ (austenite) fraction, and pitting corrosion equivalent resistance (PREN) ranges from 35 to 40 (Capello *et al.*, 2002; IMOA, 2014).

DSS is generally considered a difficult-to-cut material due to its high work hardening rate, low thermal conductivity, high ductility, and built-up edge (BUE) formation. The low thermal conductivity causes a high heat concentration in the cutting region, increasing the temperature and tool failures (plastic deformation, crater wear, and notch wear). The high work hardening increases the specific cutting pressure (k_s) that grows the machining forces and cutting power (Gowthaman *et al.*, 2020). These material properties (low thermal conductivity and high ductility) result in chips with higher shear strength, making it difficult to break them (Gamarra, 2017). Furthermore, DSS has a structure formed by Fe-α and Fe-γ (50-50) where grains of different hardness can coexist side by side; thus, the tool alternates the cutting between soft and hard grains, tending to cause a self-excited vibration (chatter) during the machining (Koyee *et al.*, 2014).

In addition to the specific cutting pressure (k_s), the machining forces are directly affected by the cutting parameters in the end milling process. Gowthaman *et al.* (2020) mentioned that low cutting speeds (v_c) combined with high feed rates (f) or high axial cutting depths (a_p) promote higher cutting forces and vibrations. Okada *et al.* (2014) found that vibration and temperature at the cutting edge are more affected by increasing feed per tooth (f_z) and axial depth of cut (a_p) than by increasing v_c in the end milling of stainless steel AISI 304. In dry cutting, low v_c favored the appearance of BUE, which did not occur with the application of the minimum quantity lubrication (MQL).

The effects of tool nose radius (r_ε) on the cutting force in dry face milling of 20%SiCp/Al composites were investigated by Niu *et al.* (2021). The results showed that, with the increase of tool nose radius, the ploughing effect between the arc cutting edge and the workpiece rose, enhancing the material deformation and specific cutting pressure (k_s), resulting in growing all machining force components. Using r_ε = 2 mm, the axial force was 3-times greater than with r_ε = 0.5 mm. However, Kuram (2017) observed in the study of AISI 304 material with cutting tools with three different tool nose radii and cutting speeds in both down and up milling. The authors found that all machining force components and the resultant force reduced with the tool-nose radius increase, regardless of the milling direction and cutting speed.

One way of evaluating the machinability of material is through the cutting forces generated in the process. In general, the higher the force involved, the greater the difficulty in machining the material (Barbosa, 2014). The static portions are characteristics in the time domain and consider the sample mean of the signal over the time interval. The time-domain analysis establishes the nature and magnitude change of the static portion, while the frequency-domain analysis demonstrates the dynamic force response to cutting conditions and the wear levels accumulated in the tool (Dimla, 2000).

Response Surface Methodology (RSM) is widely used, optimizing engineering tests and trials. One way to carry out structured planning is through the Box-Behnken Design (BBD). The BBD is an incomplete factorial rotational design introduced in 1960 by George E. P. Box and Donald W. Behnken. BBD is a statistical optimization method that aims to obtain the best results in a set of factors that influence a process. In this experimental design (DOE), each controllable factor has three levels, and the experimental points are distributed by the same distance from the central point (-1, 0, +1) (Gomes, 2013; Policena *et al.*, 2018; Garcia *et al.*, 2019). As an advantage, this DOE reduces the number of runs required and the possibility of defining the significance of each controllable input factor in the response output variables.

Thus, an attempt was made to investigate via BBD the influence of four controllable factors (cutting speed, feed per tooth, axial depth of cut, tool nose radius) and their interactions on the response variables (static and dynamic portions of the active and passive forces) in the flood end milling of duplex stainless steel UNS S32205. It is noteworthy that the influence of the tool nose radius on milling processes lacks information in the literature, supporting the present study.

2. MATERIAL AND METHODS

The chemical composition of duplex stainless steel UNS S32205 sheets supplied by Outokumpu company (Finland) was obtained by the BRUKER Q2 ION atomic emission spectrometer and compared with the ASTM A240 standard. Table 1 presents the results of the analyzes performed.

Table 1. Chemical composition of UNS S32205 (%wt.)

	C	**Si**	**Cr**	**Ni**	**Mo**	**Mn**	**Cu**	**N**	**P**	**S**
Measured	0.05	0.39	20.7	5.45	3.91	1.80	0.19	<0.005	0.024	0.01
ASTM A240	0.03 max	1.0 max	22.0-23.5	4.5-6.5	3.0-3.5	2.0 max	1.0 max	0.14-0.20	0.03 max	0.02 max

The chemical composition shows that the carbon content (%C) is higher and the chromium content (%Cr) is lower than the standard. Note that these values are performed by measuring three different locations on the plates. The material may have grades below those specified or likely a measurement factor associated with the spectrometer calibration. The lower %Cr can interfere in the Schaeffler diagram linked to the final amounts of austenite (Fe-γ) and ferrite (Fe-α). Cr is an alphagenic element, and its reduction can increase the amount of austenite in the alloy (Aguiar, 2012).

Metallographic analyzes were performed at UNS S32205 with a Zeiss Scope A1 optical microscope. The specimens were prepared with Behara's etching (80 ml distilled water, 20 ml hydrochloric acid, 1.0 g potassium metabisulfite, 200 mg ammonia bi-fluorite). Figure 1 shows the microstructure composed of austenite and ferrite. The image indicates an equilibrium between the two phases with Fe-γ arranged in elongated grains intercalating with the Fe-α matrix.

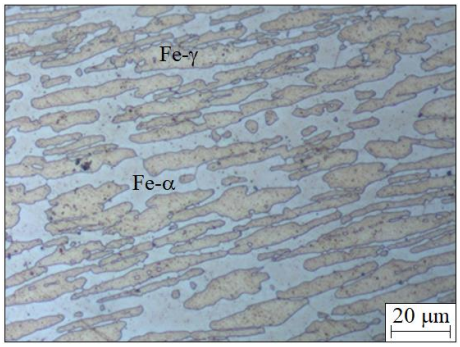

Figure 1. Microstructure of UNS S32205 (500x magnification)

The end milling was executed in rectangular plates (100 x 90 x 6 mm) with holes for fixing at the piezoelectric dynamometer. The Romi Discovery 308 machining center (4000 rpm maximum spindle and 5.5 kW maximum power) was used. In each plate, six 34 mm runs were performed applying different combinations of input factors (cutting speed "v_c", feed per tooth "f_z", axial depth of cut "a_p", tool nose radius "r_ε") through Box-Behnken Design (BBD) using statistical software Minitab 19. A Walter Tools F4042R.W20.02 milling head with 20 mm nominal diameter and support for two Walter Tools ADTM10 WSM35 TiAlN + Al_2O_3 PVD-coated carbide inserts was used. Inserts are ISO S/M class intended for machining heat-resistant superalloys and stainless steels. Three different nose radius (0.4, 0.8, 1.2 mm) were applied in the experiment. The run-out (δ) was verified for each tool assembly change with a Digimess dial gauge (0.01 mm resolution). The measured values were $\delta \leq 0.02$ mm. During the machining, a Bondmann BD-Fluid B90 oil-free bio-lubricant was used in the abundance condition (20 l/min flow rate). Fig. 2 shows the experimental setup.

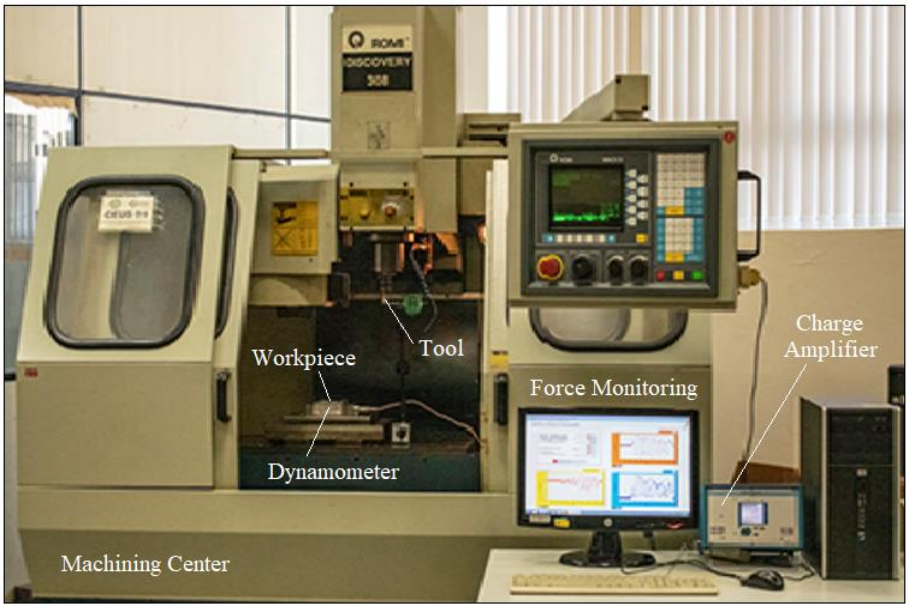

Figure 2. Experimental setup

During each run, the orthogonal components of the machining force (F_x, F_y, F_z) were collected through a Monitor System consisting of the Kistler 9129AA piezoelectric dynamometer (analog signal acquisition) fixed on the machine table, the Kistler 5070A charge amplifier (analog signal conditioning), and a dedicated computer with the Measurement Computing PCIM-DAS 1602/16 data acquisition board (A/D conversion) and LabView 9.0 software (digital signal processing). Data acquisition times were estimated according to the cutting times calculated as a function of the cutting parameters. The data acquisition rates by the DAQ board were defined based on the tool rotation, i.e., 180 points per revolution. Furthermore, the signals were monitored by LabView in the time domain during the process. The analysis and post-processing of force data were performed using Excel software.

The active force can be expressed as the resultant of the cutting force (F_c) and feed force (F_f) in end milling, as the contact angle of the tool with the workpiece (φ) constantly varies during the process. However, the active force can also be expressed by the component analysis in the orthogonal directions F_x and F_y according to Eq. (1). On the other hand, the passive force represents the projection of the machining force in a plane perpendicular to the work plane and does not contribute to the machining power, coinciding with the force exerted on the *Z*-axis according to Eq. (2).

$$F_a = \sqrt{F_c^2 + F_f^2} = \sqrt{F_x^2 + F_y^2} \tag{1}$$

$$F_p = F_z \tag{2}$$

The magnitude of the static portion (μF) is interpreted as an average value within a specified time domain of the sampled data to establish the machining force component. On the other hand, the dynamic portion (ΔF) is associated with the oscillatory components analyzed in the frequency domain of this sample (Dimla, 2000). Thus, the static portion expresses the mean value of the force (F_a or F_p) considering the sampling interval that excludes the unstable regions of entry and exit of the end-milling cutter, Eq. (3), while the dynamic portion constitutes the force fluctuation (Eq. 4).

$$\mu F = \frac{\sum_{i=1}^{N} F_i}{N} \tag{3}$$

$$\Delta F = \pm\, t_{0.95} \sqrt{\frac{\sum_{i=1}^{N} \left(F_i - \mu F\right)^2}{N}} \tag{4}$$

Where: N = number of points in the stable sampling interval; $t_{0.95}$ = 1.96 (value for a 95% confidence interval).

Table 2 shows the manageable input variables. Then, using the Minitab 19, the parameters were combined and randomized, as shown in Table 3. Subsequently, the Analysis of Variance (ANOVA) was performed.

Table 2. Coded and natural levels of BBD factors

Factors	**Unit**	**Independent Variable Levels**		
		Low (− 1)	Medium (0)	High (+ 1)
v_c	m/min	80	95	110
f_z	mm/tooth	0.06	0.12	0.18
r_ε	mm	0.4	0.8	1.2
a_p/r_ε	-	0.5	1.0	1.5

3. RESULTS AND DISCUSSIONS

Table 3 and Figures 3 and 4 illustrate the values for the static and dynamic portions of active ($\mu F_a \pm \Delta F_a$) and passive ($\mu F_p \pm \Delta F_p$) forces during the end milling of duplex stainless steel UNS S32205 for 27 combinations determined by BBD.

Table 3. Force values measured during the milling UNS 32205

Run	**Controllable Factors**					**Response Variables**			
	v_c (m/min)	f_z (mm/z)	a_p (mm)	r_ε (mm)	$\frac{a_p}{r_\varepsilon}$	F_a (N)		F_p (N)	
						μFa	$\pm \Delta F_a$	μF_p	$\pm \Delta F_p$
1	95	0.12	0.2	0.4	0.5	81.2	56.6	105.4	37.9
2	95	0.06	1.2	0.8	1.5	249.5	162.7	76.3	47.2
3	80	0.12	1.2	1.2	1.0	136.7	87.0	96.6	50.4
4	110	0.12	0.4	0.8	0.5	132.1	80.1	102.8	43.4
5	95	0.18	1.2	1.2	1.0	466.6	305.5	156.4	87.1
6	95	0.06	0.4	0.4	1.0	91.5	110.1	73.7	50.4
7*	95	0.12	0.8	0.8	1.0	264.0	194.03	97.3	65.3
8	80	0.12	0.4	0.8	0.5	133.1	107.5	95.3	62.6
9	**95**	**0.18**	**1.2**	**0.8**	**1.5**	**291.0**	**581.1**	**30.6**	**121.2**
10	80	0.12	1.2	0.8	1.5	378.4	233.1	123.8	48.3
11	95	0.12	0.6	0.8	0.5	185.3	124.4	115.8	60.7
12	110	0.12	0.4	0.4	1.0	136.7	87.0	96.6	50.4
13	110	0.12	1.2	0.8	1.5	811.2	371.1	199.4	62.6
14	95	0.18	0.4	0.4	1.0	182.3	106.7	116.2	62.8
15	95	0.12	0.6	0.4	1.5	281.3	198.7	142.4	63.5
16*	95	0.12	0.8	0.8	1.0	269.3	168.7	132.7	67.2
17	80	0.12	0.4	0.4	1.0	136.5	87.4	55.5	48.0
18	95	0.06	1.2	1.2	1.0	245.3	177.7	111.8	64.0
19	95	0.12	1.8	1.2	1.5	522.8	310.5	135.2	53.9
20	95	0.18	0.4	0.8	0.5	165.2	120.0	107.7	71.0

* Runs at the medium significance level of the controllable input factors.

Table 3. Cont.

Run	Controllable Factors					Response Variables			
	v_c (m/min)	f_z (mm/z)	a_p (mm)	r_ε (mm)	$\frac{a_p}{r_\varepsilon}$	F_a (N)		F_p (N)	
						μFa	$\pm \Delta F_a$	μF_p	$\pm \Delta F_p$
21	110	0.18	0.8	0.8	1.0	567.5	360.9	238.7	152.0
22	95	0.06	0.4	0.8	0.5	266.8	273.6	92.4	71.7
23	110	0.12	1.2	1.2	1.0	379.7	201.7	156.1	51.1
24	110	0.06	0.8	0.8	1.0	110.0	135.1	75.1	53.1
25*	95	0.12	0.8	0.8	1.0	274.1	186.5	108.2	61.4
26	80	0.06	0.8	0.8	1.0	195.5	121.5	91.8	46.6
27	80	0.18	0.8	0.8	1.0	382.2	312.2	114.0	73.7

* Run at the medium significance level of the controllable input factors.

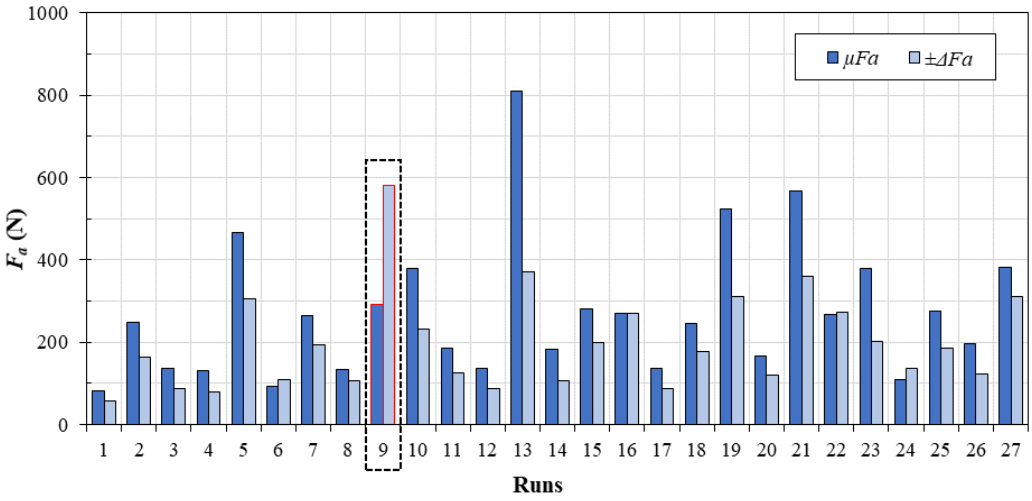

Figure 3. Static and dynamic portions of active forces

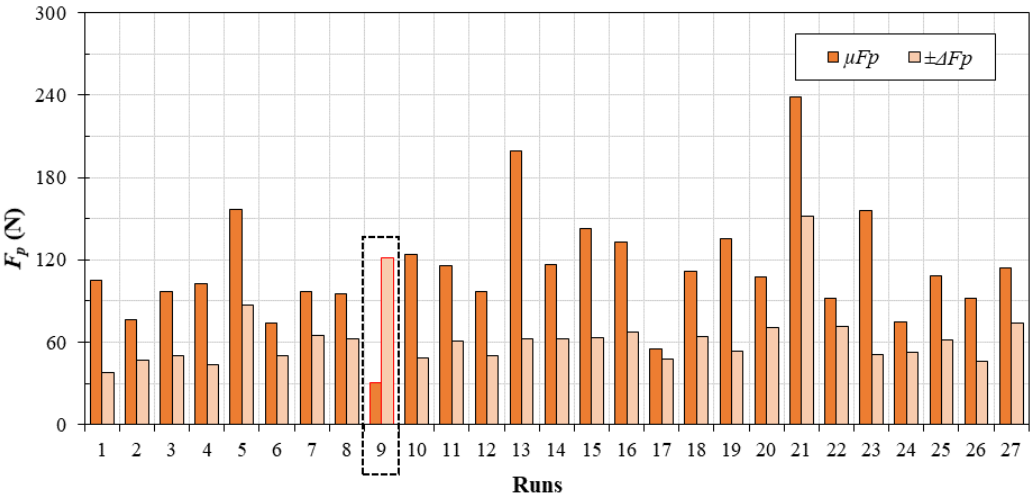

Figure 4. Static and dynamic portions of passive forces

Run 9 stood out in the experimentation for presenting strong instability (vibrations) in the end milling process. As a result, severe chipping on the tool edge occurred during cutting (Fig. 5). However, the data samples were considered

before fracture. In this case, the dynamic portion was higher than the static portion by 102% for F_a and 296% for F_p. Sória (2016) explains that the lower the a_p/r_ε ratio, the greater the force in the axial direction (F_p) that tends to push the tool edge away from the cutting region, tending to increase vibration. On the other hand, for a higher a_p keeping the same r_ε, the machining force (or resultant force) tends to increase its component in the radial direction (increasing F_a). As a_p/r_ε = 1.5, the cutting tool was overloaded, causing the tool failure.

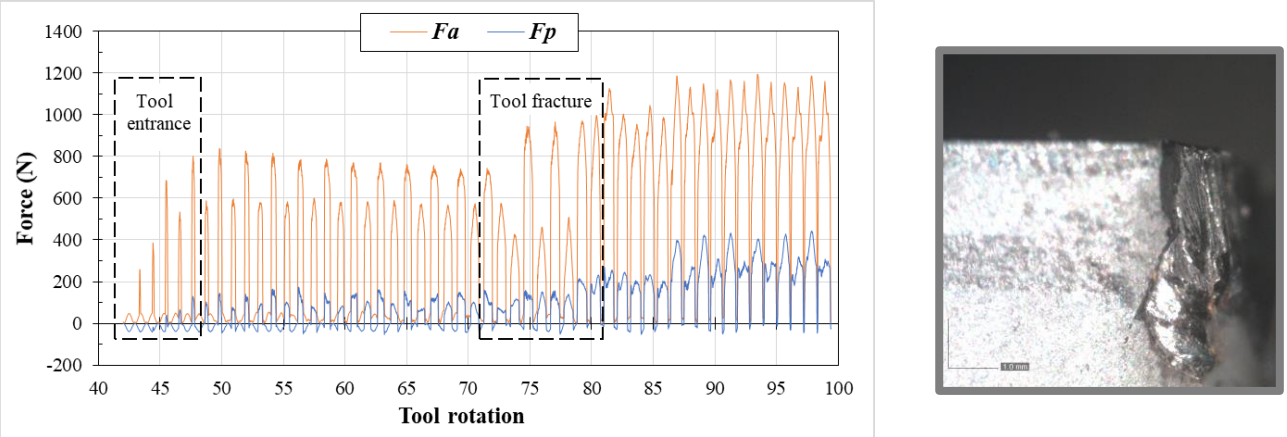

(a) (b)

Figure 5. Run 9: (a) force signals during the milling; (b) tool state after the machining

In run 9, the situation was stern because the tool nose was not robust enough, and the tool edge did not support this dynamic instability. This failure did not occur when r_ε = 1.2 mm is used, even with the same a_p/r_ε value (1.5). Comparing three runs (15, 10, 19) with high a_p/r_ε and medium f_z (0.012 mm/tooth), an increase in F_a and a reduction in F_p is associated with an increase in a_p (0.6, 1.2, 1.8 mm respectively) and r_ε (0.4, 0.8, 1.2 mm correspondingly).

Disregarding run 9, the smallest values of active force occurred during run 1 for both static (μF_a = 81.2 N) and dynamic (ΔF_a = 56.6 N) portions because it has the smallest cross-section area (Fig. 3) with a_p/r_ε = 0.5. The highest values were generated in run 13 (F_a = 811.2 ± 371.1 N) with a_p/r_ε = 1.5. Santos and Sales (2007) explain that by increasing feed per tooth (f_z) and depth of cut (a_p), the forces rise directly, almost linear, due to the increase in primary and secondary shear zones during cutting. Moreover, according to Kuram (2017), all force components (F_x, F_y, F_z) increase with decreasing r_ε and thus with increasing the a_p/r_ε ratio. However, all input parameters affect directly or indirectly these forces. Fig. 4 exhibits that run 17 generated the lowest value of passive force for the static portion (μF_p = 55.5 N). The lowest dynamic portion was also measured in run 1 (ΔF_p = 37.9 N). In these runs (1 and 17), r_ε = 0.4 mm was used. The highest values of μF_p (238.7 N) and ΔF_p (152.0 N) were obtained on the run 16 with a_p/r_ε = 1.0. Therefore, it was noted that the a_p/r_ε ratio has different effects on the active and passive milling forces.

In three other runs (6, 22, 24), the dynamic portion of the active force was higher than the static portion ($\Delta F_a > \mu F_a$), which indicates high force fluctuation, and these runs were with the same level of f_z (0.06 mm/tooth). Thus, the dynamic portion is about 20% larger than the static portion in run 6, while the percentual increase was minor (2.5%) in run 22. At run 24, the rise was approximately 23%. Note that runs 6 and 22 used the same cutting parameters (v_c, f_z, a_p) differing only in the tool nose radius used (0.4 mm and 0.8 mm, respectively), resulting in a smaller a_p/r_ε ratio and larger values of F_a and F_p in run 22. In this case, the ploughing effect between the arc cutting edge and the workpiece rises by increasing r_ε, resulting in higher force values (Niu *et al.*, 2021). However, there were no instabilities during these three runs.

The literature presents a lack of information that addresses the a_p/r_ε ratio. It is known that this ratio influences the amplitude of the axial (passive) and radial forces due to the forces decomposition in end milling. Considering medium a_p/r_ε (1.0) and maximum f_z (0.18 mm/tooth) with a variation of v_c, ΔF_p represents a smaller percentage of about μF_p for the highest r_ε (1.2 mm). Thus, one hypothesis is that the increase in the a_p/r_ε ratio decreases the passive force for an average cutting section since the cutting speed deviates from the natural system frequency.

Table 3 presents the results obtained with the reduced variance analysis (ANOVA) of the active and passive forces. The values in bold refer to the significant factors on the response variables for a 95% confidence interval, while the values in gray represent the partially significant factors (90.0% to 94% confidence interval). The *Prop*. (%) column indicates the contribution percentage of the term in the model relative to the total sum of squares.

The results have shown that the linear effects of the controllable factors f_z, r_ε, and a_p/r_ε were significant for the static and dynamic portions of the active force (μF_a and ΔF_a). Furthermore, the interaction f_z x a_p/r_ε and the quadratic effects of f_z and r_ε were also significant for ΔF_a. Besides, the interaction v_c x a_p/r_ε was partially significant for μF_a and ΔF_a. Regarding the passive force, f_z and its interaction with v_c were partially significant for μF_p and significant for ΔF_p. The

static portion of the passive force was also partially influenced by the linear effects of v_c and r_ε, and the dynamic portion was significantly influenced by f_z x f_z and f_z x a_p/r_ε.

Table 3. Reduced ANOVA for the analyzed variables

Factor	μF_a		$\pm \Delta F_a$		μF_p		$\pm \Delta F_p$	
	p-value	Prop. (%)	p-value	Prop. (%)	p-value	Prop. (%)	p-value	Prop. (%)
v_c	0.241	2.68	0.485	0.23	**0.098**	8.77	0.386	1.27
f_z	**0.030**	9.05	**< 0.001**	15.05	**0.076**	10.27	**< 0.001**	30.32
r_ε	**0.003**	19.45	**< 0.001**	12.95	**0.068**	10.89	0.117	4.36
a_p/r_ε	**0.001**	27.80	**< 0.001**	27.79	0.499	1.36	0.373	1.34
v_c x v_c	0.177	3.22	-	-	0.261	5.21	-	-
f_z x f_z	-	-	**0.008**	4.98	0.438	1.80	**0.010**	13.67
r_ε x r_ε	-	-	**0.025**	4.23	-	-	-	-
a_p/r_ε x a_p/r_ε	-	-	-	-	-	-	-	-
v_c x f_z	0.233	2.48	-	-	**0.073**	10.48	**0.034**	8.51
v_c x r_ε	-	-	-	-	0.514	1.27	0.257	2.21
v_c x a_p/r_ε	**0.064**	6.36	**0.058**	1.90	0.369	2.43	0.297	1.85
f_z x r_ε	-	-	0.124	1.20	-	-	-	-
f_z x a_p/r_ε	0.523	0.69	**< 0.001**	22.75	0.420	1.95	**0.028**	9.21
r_ε x a_p/r_ε	0.539	0.64	-	-	-	-	-	-
Error		6.69		7.27		45.56		27.25
R^2	72.4%		92.6%		54.4%		72.7%	

The coefficients of determination (R^2) presented different values. The values concerning the active force (static and dynamic portions) and the dynamic portion of the passive force are above 70%. According to Montgomery (2007), these models are adjusted to the data. However, for the static portion of the passive force, the value of R^2 for the active portion is below 70%, indicating that the model data can show high variability.

Contour plots were generated to visualize the relationship of the active (Fig. 6) and passive (Fig. 7) forces with the controllable input factors.

Concerning the static portion of active force (Fig. 6a), for v_c = 95 m/min and r_ε = 0.8 mm (medium levels), a decrease in μF_a occurs when f_z and a_p reduce concurrently. Figure 6b shows that, for v_c = 95 m/min and a_p/r_ε = 1 (medium levels), the lower values of ΔF_a are generated when r_ε = 0.4 mm and $f_z \leq$ 0.12 mm/tooth.

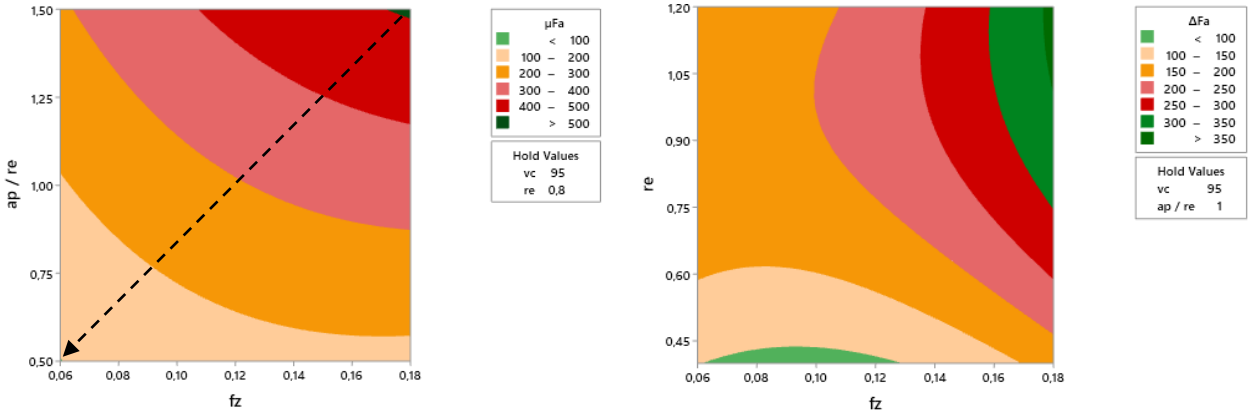

(a) μF_a (b) ΔF_a

Figure 6. Contour plots of active force ($\mu F_a \pm \Delta F_a$)

Regarding the static portion of active force (Fig. 7a), for r_ε = 0.8 mm and a_p/r_ε = 1 (medium levels), the lower values of μF_p are generated when fz = 0.06 mm/tooth and 97 m/min < v_c < 108 m/min. For ΔF_p (Fig. 7b), when considering v_c = 95 m/min and r_ε = 0.8 mm (medium levels), there is a region delimitated by f_z < 0.09 mm/tooth and a_p > 1.2 mm.

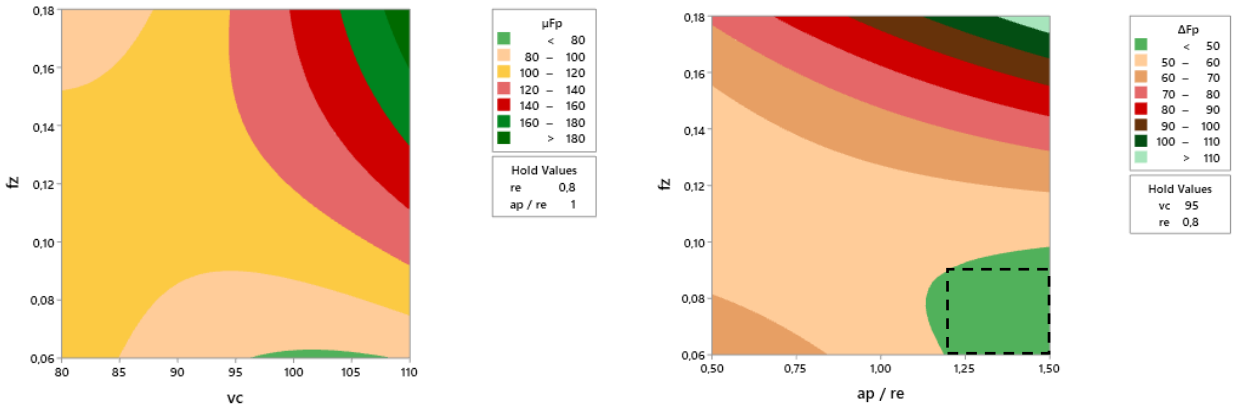

(a) μF_p (b) ΔF_p

Figure 7. Contour plots of passive force ($\mu F_p \pm \Delta F_p$)

The analyses specified above produced the contour plots based on the adopted input parameters' levels. The influence of the main factors on the behavior of the forces was evaluated. Smaller force values resulted from low levels of axial depth of cut and feed per tooth. These combinations correspond to a smaller cross-section, which agrees with the theory presented in this study and the results obtained through ANOVA. The influence of the cutting speed on μF_a could also be seen. On the other hand, there was no influence from v_c on ΔF_p generated during the end milling of UNS S32205.

After analyzing the active and passive force values, the best controllable factor arrangement was determined to optimize the response variables (smaller-is-better). Each response (y) was minimized aided by Minitab 19 within the range of parameters established in this work. Figure 8 shows the controllable input factors optimized to simultaneously minimize the Fa and Fp values (multivariate optimization).

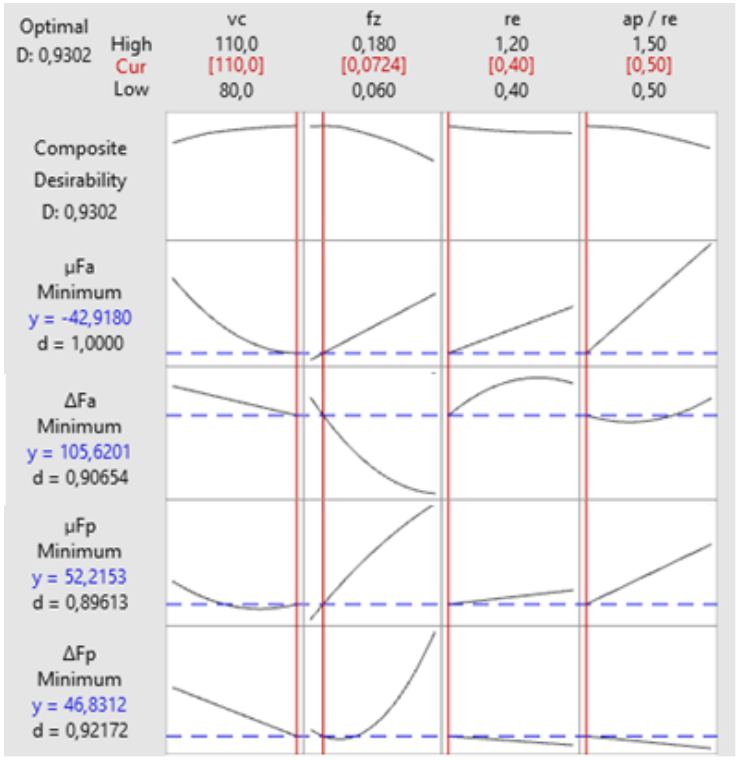

Figure 8. Multivariate optimization

The optimal levels of the parameters (within the applied limit values) were determined (v_c = 110 m/min, f_z = 0.072 mm/tooth, r_ε = 0.4 mm and a_p = 0.2 mm) in order to minimize the response variables simultaneously (μF_a, ΔF_a,

μF_p, ΔF_p). The function "D" (composite desirability) indicates the desired value of the predicted data for the combined variables: the closer to 1.0, the greater the probability that they will be obtained. In this work, the value D = 0.9306. The estimated values for the response variables through the model were $F_a = -42.9 \pm 105.6$ N and $F_p = 52.2 \pm 46.8$ N. It is intended to do out the runs to validate these results later.

4. CONCLUSIONS

The present work investigated the influence of four controllable factors (cutting speed v_c, feed per tooth f_z, axial depth of cut a_p, and tool nose radius r_ε) and their interactions on the response variables (static and dynamic portions of the active and passive forces) during the flood end milling of duplex stainless steel UNS S32205 through the Box-Behnken Design (BBD). The main conclusions were:

- The lowest value of active force ($F_a = 81.2 \pm 56.6$ N) occurred in run 1 ($v_c = 95$ m/min, $f_z = 0.12$ mm/tooth, $a_p = 0.2$ mm, and $r_\varepsilon = 0.4$ mm) because it has the smallest cross-section area.
- The highest value ($F_a = 811.2 \pm 371.1$ N) was generated in run 13 ($v_c = 110$ m/min, $f_z = 0.12$ mm/tooth, $a_p = 1.2$ mm, and $r_\varepsilon = 0.8$ mm), which the increment of the depth of cut (a_p) causes the rising of force.
- Run 17 ($v_c = 80$ m/min, $f_z = 0.12$ mm/tooth, $a_p = 0.4$ mm, and $r_\varepsilon = 0.4$ mm) generated the lowest value of the static portion ($\mu F_p = 55.5$ N) of the passive force. The lowest dynamic portion ($\Delta F_p = 37.9$ N) was also generated by run 1. In both runs (1 and 17), it was used $r_\varepsilon = 0.4$ mm.
- The highest value of passive force ($F_p = 238.7 \pm 152.0$ N) occurred on the run 16 ($v_c = 95$ m/min, $f_z = 0.12$ mm/tooth, $a_p = 0.8$ mm, and $r_\varepsilon = 0.8$ mm).
- Run 9 ($v_c = 95$ m/min, $f_z = 0.18$ mm/tooth, $a_p = 1.2$ mm, and $r_\varepsilon = 0.8$ mm) showed strong vibrations in the end milling process. As a result, there was chipping of the tool edge during cutting. In this case, it was observed that the dynamic portion was significantly higher than the static portion ($\Delta F > \mu F$) by 102% for F_a and 296% for F_p.
- BBD and ANOVA showed that r_ε, a_p/r_ε and f_z are the most significant variables on the static and dynamic portions of the active and passive force. However, diverse combinations of the four input parameters affect the response variables.
- The optimized controllable factors to generate the lowest F_a and F_p values were: $v_c = 110$ m/min, $f_z = 0.072$ mm/tooth, $r_\varepsilon = 0.4$ mm, and $a_p = 0.2$ mm. Therefore, the estimated values were $F_a = -42.9 \pm 105.6$ N and $F_p = 52.2 \pm 46.8$ N.

5. ACKNOWLEDGEMENTS

The authors thank Outokumpu Co. for donating the material; Walter Tools Co. for the tools; Bondmann Chemistry Co. for the cutting fluid; Foundry Laboratory (LAFUN-UFRGS) for the chemical composition analysis; UPF-Parque for the metallographic analysis.

6. REFERENCES

Aguiar, D.J.M., 2012. *Study of Deformation-Induced Martensite Formation and Reversion in the Austenite of Two Duplex Stainless Steels.* Master's Thesis in Metallurgical and Materials Engineering, POLI-USP, São Paulo, Brazil (in Portuguese).

Barbosa, P.A., 2014. *Study of Mechanic Behavior in Stainless Steel Machining*. Master's Thesis in Mechanical Engineering, POLI-USP, São Paulo, Brazil (in Portuguese).

Capello, E., Chiarello, P., Previtali, B. and Vedani, M., 2003. "Laser welding and surface treatment of a 22Cr-5Ni-3M0 duplex stainless steel". *Materials Science and Engineering: A*, Vol. 351, No. 1-2, pp. 334-343.

Dimla, D.E., 2000. "Sensor signals for tool-wear monitoring in metal cutting operations – a review of methods". *International Journal of Machine Tools and Manufacturing*, Vol. 40, No. 8, pp. 1073-1098.

Diniz, A.E, Marcondes, F.C. and Coppini, N.L. 2013. *Tecnologia da Usinagem dos Materiais.* 8.ed. Editora Artliber, São Paulo.

Gamarra, J. R. 2017. *Machining Strategies in Super Duplex Stainless Steel Turning* (*UNS S32750*). Master's Thesis in Mechanical Engineering, FEM-UNICAMP, Campinas, Brazil (in Portuguese).

Garcia, R.F., 2019. *Comparative Analysis of Finish Face Milling in Duplex Stainless Steels DX 2205 and LDX 2101*. Master's Thesis in Mechanical Engineering, PROMEC-UFRGS, Porto Alegre, Brazil (in Portuguese).

Garcia, R.F., Feix, E.C., Mendel, H.T., Gonzalez, A.R. and Souza, A.J., 2019. "Optimization of cutting parameters for finish turning of 6082-T6 aluminum alloy under dry and RQL conditions"**.** *Journal of the Brazilian Society of Mechanical Sciences and Engineering*, Vol. 41, Art. 317.

Gomes, S.V.F., 2013. *Application of Box-Behnken Design to Optimize Flavonoid Extraction Method Using Accelerated Solvent Extraction (ASE) and Quantification of Chemical Markers by CLAE-DAD-UV in Species of the Genus Passionflower*. Ph.D. Thesis in Organic Chemistry, UFBA, Salvador, Brazil (in Portuguese).

Gowthaman, P.S., Jeyakumar, S. and Saravanan, B.A. 2020. "Machinability and tool wear mechanism of duplex stainless steel –A review". *Materials Today: Proceedings*, Vol. 26, Part 2, pp. 1423-1429.

IMOA, 2014. *Practical Guidelines for the Fabrication of Duplex Stainless Steels***.** 3 ed. International Molybdenum Association Pittsburgh: TMR Stainless.

Koyee, R.D., Eisseler, R. and Schmauder, S. 2014. "Application of Taguchi coupled fuzzy multi-attribute decision making (FMADM) for optimizing surface quality in turning austenitic and duplex stainless steels". *Measurement*, Vol. 58, No. 1, p. 375-386.

Kuram, E. 2017. "Nose radius and cutting speed effects during milling of AISI 304 material". *Materials and Manufacturing Processes*, Vol. 32, No. 2, p. 185-192.

Niu, Q., Jing, L., Li, C., Yu, Z., Li, S., Li, P., Qiu, X., Ko, T., Yue, W. 2021. "Study on effects of tool nose radius on the formation mechanism of edge defects during milling SiC_p/Al composites". *The International Journal of Advanced Manufacturing Technology*, Vol. 114, N. 5-8, p. 2261-2269.

Okada, M., Hosokawa, A., Asakawa, N., Ueda, T., 2014. "End milling of stainless steel and titanium alloy in an oil mist environment". *The International Journal of Advanced Manufacturing Technology*, Vol. 74, pp. 1255-1266.

Policena, M.R., Devitte, C., Fronza, G., Garcia, R.F. and Souza, A.J., 2018. "Surface roughness analysis in finishing end-milling of duplex stainless steel UNS S32205". *The International Journal of Advanced Manufacturing Technology*, Vol. 98, N. 5-8, p. 1617-1625.

Santos, S.C.; Sales, W.F. 2017. *Aspectos Tribológicos da Usinagem dos Materiais*, Editora Artliber, São Paulo.

Sória, B.S. 2016. *Study of Vibration Behavior in Face Milling of AISI 316 Stainless Steel Using Wavelet Transform.* Master's Thesis in Mechanical Engineering, PROMEC-UFRGS, Porto Alegre, Brazil (in Portuguese).

RESPONSIBILITY NOTICE

The authors are the only ones responsible for the printed material included in this paper.